This paper was published in Nature Geoscience

PUBLISHED ONLINE: 22 JANUARY 2012 | DOI: 10.1038/NGEO1379

The published version can be found at

http://www.nature.com/ngeo/journal/vaop/ncurrent/full/ngeo1379.html

Western Arctic Ocean freshwater storage increased by wind-driven spin-up of the Beaufort Gyre

Katharine A. Giles[1*], Seymour W. Laxon[1], Andy L. Ridout[1], Duncan J. Wingham[1] & Sheldon Bacon[2]

[1]Centre for Polar Observation and Modelling, Department of Earth Sciences, University College London, Gower Street, London WC1E 6BT, UK.

[2]National Oceanography Centre, Southampton, University of Southampton, Waterfront Campus, European Way, Southampton, SO14 3ZH, UK.

*Corresponding author

Email: katharine.giles@ucl.ac.uk

Telephone: +442076794450

Fax: +442076797883

Introduction

The Arctic Ocean's freshwater budget comprises contributions from river runoff, precipitation, evaporation, sea-ice and exchanges with the North Pacific and Atlantic[1]. The consequent storage of >70,000 km^3 of freshwater[2] reduces the salinity of upper-layer seawater, which is separated from underlying warm, saline water by a strong halocline. Spatially and temporally limited observations show that the Arctic Ocean's freshwater content increased over the last few decades, predominantly in the west[3,4,5], and that freshwater entering the North Atlantic decreased by a similar amount[6]. Models suggest that wind-driven convergence drives freshwater accumulation[7], but there are no continuous observations of changes in sea surface height (SSH) or halocline depth associated with this mechanism. Here we show the wind-driven spin-up of the Beaufort Gyre from continuous satellite measurements of SSH between 1995-2010. We observe a positive SSH trend and show that the trend in the wind field has a corresponding spatial pattern, indicating that wind-driven convergence controls freshwater variability. We calculate a freshwater increase of 8000±2000 km^3 over the Western Arctic, in keeping with hydrographic observations[4,5]. A reversal in the wind field could spin-down the Beaufort Gyre, releasing this freshwater to the Arctic Ocean and/or the North Atlantic, potentially affecting the wider global ocean circulation[8].

Main

The Canada Basin contains the largest proportion of the Arctic Ocean's freshwater with the majority located in the Beaufort Gyre[2] (figure 1a), a permanent anti-cyclonic circulation system. Comparisons between the Beaufort Gyre climatology, derived from winter data collected between 1950 and 1989, and an aerial hydrographic survey from March-April 2008 containing 64 station locations over ~560,000 km^2, suggest that the Beaufort Gyre freshwater content has increased by 8500 km^3 [4](the uncertainty was not estimated). A similar increase of 8400±2000 km^3 was found over the whole Arctic Ocean from analysis of Conductivity-Temperature-Depth (CTD) and Expendable CTD observations from ships, submarines and ice drifting stations between the 1990s and 2006-2008[5], with the results also "hinting"[5] at a shift and expansion of the Gyre. However, as sampling is biased towards summer months, only observations between July-September were used[5]. Simultaneously, combined analysis of hydrographic data collected between 1990-2008 and coupled sea-ice-ocean general circulation model indicate that freshwater export through Davis Strait reduced by ~50%, comparable to the observed increase in storage[6]. To use these snapshots of freshwater change to understand its variability and governing physics, models must be employed to put them into context. The wind exerts a frictional force on the ocean surface and ocean surface waters respond to balance this force with the Coriolis force. This motion is termed Ekman transport. Variations in the magnitude and direction of the wind cause spatial gradients in the Ekman transport, and water to accumulate or dissipate, changing the SSH and depth of the halocline. The resulting vertical velocity of the SSH or halocline is termed Ekman pumping. Modelling experiments suggest that freshwater is accumulated in the Beaufort Gyre during anticyclonic regimes and forced to the Arctic Ocean margins during cyclonic regimes, where it may then be released to the North Atlantic[7]. Therefore, the storage of freshwater in the Beaufort Gyre is predicted to vary with the wind stress curl. This is supported by data collected between 2003-2007 at two moorings in the Beaufort Sea that show an increase in the freshwater content and a strong negative wind stress curl over the same period[3].

Here we present the trend in the SSH (figure 1b) between 1995-2010, from which we calculate the change in the freshwater storage (figure 3), and a corresponding trend in the wind field curl $\nabla \times \mathbf{u}|\mathbf{u}|$ (a measure of the spatial gradients in the wind that give rise to Ekman convergence or divergence), where $\mathbf{u}$ is the wind vector (figure 1c). The trend in the SSH is derived from continuous satellite radar altimetry data from the Earth Remote Sensing (ERS2) (1995-2003) and Envisat (2002- 2010) satellites (figure 1b). Our data cover the Arctic region between 70°N-81.5°N, the latitudinal limit of the satellites, covering the majority of the Canada Basin and therefore, the Beaufort Gyre.

The trend in SSH (figure 1b) shows an increase in the doming of the Beaufort Gyre: the trend in the SSH is greater in the centre of the Gyre than around the edge. The maximum increase of 2.00±0.05 $cmyr^{-1}$ is centred on 78.9° N, 159.4° W. The average increase over the Western Arctic (70°-81.5° N, 130°-180° W) is 1.15±0.04 $cmyr^{-1}$. The pattern of the trend (figure 1b), when compared to the map of the mean SSH (figure 1a), shows that the Beaufort Gyre has also expanded towards the north-west over this period. However, the individual annual maps of the SSH (not shown here) show that the centre of the gyre has remained between 72.4°-74.4° N and 139°-151° W. For comparison, in-situ observations have placed the centre of the gyre around 73.5° N, 143° W since the 1990s[3]. The changes are limited to the Western Arctic. Excluding data from this area, we calculate an average SSH trend of 0.25±0.04 $cmyr^{-1}$ north of 70° N, which is similar to the ~0.2 $cmyr^{-1}$ estimated from tide gauge data in the coastal areas of the Russian Arctic between 1954 and 1989[9].

Over the Beaufort Gyre, the trend in the wind field curl (figure 1c) shows a very similar spatial pattern to the trend in the SSH (r=-0.9 over the Western Arctic as defined above). This correlation is not observed in shallow and coastal areas of the Arctic (e.g. the Canadian Archipelago) where the ocean is constrained by topography unlike the deep Canada Basin.

The variability in the SSH over the Western Arctic (figure 2), with respect to the 15-year mean SSH (figure 1a), reveals that the trend (1.88±0.09 $cmyr^{-1}$) between 2002 and 2010 was over three times larger than the trend (-0.59±0.13 $cmyr^{-1}$) between 1996 and 2002 (N.B. annual averages are computed between September and August the following year. Reference to these averages uses the later year: e.g. 1996 refers to September 1995 to August 1996).

We calculate in consequence that the Beaufort Gyre's surface geostrophic velocity (the velocity of the current driven by the pressure gradient) was almost three times greater by 2010 than it was between 1996-2002. Between 1996-2002 it was 1.90±0.10 cms^{-1}. From the trend between 2002-2010, we calculate an increase in the geostrophic velocity of 3.60±0.03 cms^{-1}, resulting in a total geostrophic velocity of 5.50±0.10 cms^{-1} by 2010.

We estimate a change in the freshwater content (figure 3) over the Western Arctic between 1995-1996 and 2009-2010 of 8000±2000 km^3, with a maximum difference of 10,000±2000 km^3 between 2000-2001 and 2007-2008. Freshwater content changes are calculated using our SSH measurements and estimates of the change in mass from the Gravity Recovery and Climate Experiment (GRACE)[10] satellite when data are available (2002-2010). The change in freshwater content is plotted with and without removing the mass contribution to demonstrate that, over this time period in the Western Arctic, changes in mass provide a relatively small contribution to the total change in freshwater. The origin of this recently stored freshwater has been shown by tracer measurements to be from the accumulation sea ice melt water and river runoff[5].

Our results show a correlation between increasing anti-cyclonicity of the wind field and the trend in SSH and therefore accumulation of freshwater in the Beaufort

Gyre. It is possible that the marked anti-cyclonicity of the wind field during the 2000s caused the freshwater accumulation[3]. But it is also striking that the near-constant trend in the wind field over our time period (figure 2) is in distinct contrast to the SSH trends during the earlier and latter parts. Ekman pumping is not the only mechanism by which water can be redistributed. A model study[5] suggests that changes in horizontal advection and mixing can lessen the influence of Ekman pumping. However, the same model shows a close correlation between Ekman pumping and the vertical velocity of the 34-isohaline for most of its study period, indicating that changes in thickness of the wind-driven layer are due to variations in the Ekman pumping. Therefore, our results indicate that the wind is more effective at spinning up the gyre during the 2000s: the efficiency of the transfer of momentum from the atmosphere to the ocean increased. For this reason we have plotted $\nabla \times \mathbf{u}|\mathbf{u}|$ rather than the wind stress curl, which is calculated by multiplying the wind field curl by drag coefficient and density terms. There are different potential causes for an increase in the transfer of momentum. The Arctic Ocean is covered by sea ice, which contains leads (areas of open water). The wind drives the surface water directly over leads and deforms and moves the sea ice, which drives the water beneath. Buoy observations show a large ice deformation rate in summer 2007 compared to previous summers (1979-2006) suggesting that the mechanical strength of the ice decreased, making it easier to move[11]. An increased ice drift speed has also been observed from 2004-onwards, which cannot be fully explained by changes in wind speed[12]. Arctic sea ice extent and thickness are declining[13,14,15] and this decrease in ice thickness is a likely cause of the increase in ice deformation rate and drift speed[11,12]. Increasing ice deformation also results in more leads[11] and ridges, increasing the area of vertical surfaces the wind can blow against, which increases the momentum transfer to the sea ice[16]. The atmospheric momentum flux is also influenced by the turbulent fluxes of sensible and latent heat from the surface[17], which depend on the presence/thickness of the sea ice. These potential influences on the transfer of momentum between the atmosphere and the ocean might also explain why we see more interannual variability in the wind field curl than the SSH between 2002-2010.

Our results provide a basin-wide, time-continuous view of changes to the SSH revealing an increase in the freshwater content between 1995 and 2010 of 8000±2000 km^3 over the Western Arctic (similar to the 8500 and 8400±2000 km^3 observed from in-situ measurements[4,5]). The geostrophic velocity is almost three times greater in 2010, compared to the 1990s and the spatial pattern of the trend in SSH is correlated (r=-0.9) to the spatial pattern of the trend in the wind field curl providing observational evidence that Ekman transport has driven the storage of freshwater in the Beaufort Gyre between 1995 and 2010. Our results also provide a detailed picture of the year-to-year variability in the SSH and wind field curl and suggest that other factors beyond simply the change in the wind might contribute to the spin-up of the Beaufort Gyre. While these data only address changes in the Western Arctic, it is striking that our calculated increase of freshwater is similar to the ca. 10,000 km^3 of freshwater that entered the Nordic Seas from the Arctic[8] during the late 1960s and early 1970s causing the Great Salinity Anomaly (GSA)[18], influencing the production of Labrador Sea Water, which becomes upper North Atlantic Deep Water[19]. Our results suggest that a reversal of the wind field to more cyclonic conditions would result in the spin-down of the Beaufort Gyre and the consequent release of this freshwater into the rest of the Arctic Ocean and/or its exchange with adjacent oceans. Indeed, when we extend the wind field curl anomaly over the Western Arctic back in time (not shown here) it reveals that the atmospheric circulation became increasingly cyclonic between mid the 1980s and mid 1990s and hydrographic observations also show a freshening of the Nordic Seas and Subpolar Basins during this period[8,20]. Our results indicate an increase in the transfer of momentum between the atmosphere and the ocean after 2002, which could enhance the spin-up and spin-down of the Arctic Ocean. While the increase in fresh water might increase the vertical stratification of the water column in the Beaufort Gyre, we note too that increased spin-up of the Arctic Ocean might, through increased turbulence, enhance the vertical transport of heat from warm, deeper Atlantic-sourced waters to the cold upper ocean and lead to a reduction in winter ice growth, creating an additional positive feedback to the ice-albedo effect as the ice cover retreats.

Methods

Sea surface height (SSH)

Although SSH is measured by radar altimeters over the world ocean, different processing techniques must be used over ice. ERS-2 provided the first map of Arctic SSH variability[21] and the ICESat laser altimeter provided the Arctic dynamic topography for February/March, 2004-2008[22]. Our method utilises the fact that the radar observes specular echoes over leads and diffuse echoes over ice[21]. The supplementary information describes the process of calculating elevations from echoes, and the calibration between data from leads and ocean, and data from ERS-2 and Envisat.

The monthly average SSH was calculated by subtracting the EGM08 geoid[23] from the elevation data and filtering to remove outliers; data were then averaged on a 200 km grid. For each grid cell, we averaged the monthly data to calculate the mean sea surface (MSS) (figure 1a) and the SSH variability (figure 2) was calculated by computing annual MSS (September to August the following year) and subtracting the total MSS. The trend in the SSH was calculated using LINFIT (IDL), which fits data to the model, $y = a + bx$, by minimizing the chi-square error statistic (http://star.pst.qub.ac.uk/idl/LINFIT.html). It is possible that during June, July and August elevation estimates might include measurements from melt ponds, which would bias our elevations high. However, excluding these months from our data biases our trend high (by 20%) as the annual SSH cycle is not uniform. The fact that this bias is positive demonstrates that increasing melt pond fraction cannot contribute to the trend.

The uncertainty in the SSH is due to measurement, orbit, tidal, instrument noise and atmospheric propagation error along with the uncertainties in correcting for the biases between the two satellites and between measurements from the ocean and leads (see supplementary information).

Wind field curl

$$\nabla \times \mathbf{u}|\mathbf{u}| = \left(\frac{\partial (v|\mathbf{u}|)}{\partial x} - \frac{\partial (u|\mathbf{u}|)}{\partial y} \right) \hat{z} \tag{1}$$

where $|\mathbf{u}| = \sqrt{(u^2 + v^2)}$ and u and v are surface zonal and meridional winds from NCEP/NCAR Reanalysis data[24], NOAA/OAR/ESRL PSD, Boulder, Colorado, USA, (http://www.esrl.noaa.gov/psd/). Monthly averages were calculated on a 200 km grid. For each grid cell, the total mean curl was calculated by averaging all months of data and the annual anomaly was computed by subtracting the total mean curl from annual means of the monthly data.

We estimate an uncertainty of 10% in $\nabla \times \mathbf{u}|\mathbf{u}|$ from comparison with in-situ validation of wind speed estimates[25,26] (see supplementary information).

Geostrophic velocity

The geostropic balance is[27]

$$fu = -g\frac{\partial \eta}{\partial y} \quad fv = g\frac{\partial \eta}{\partial x} \tag{2}$$

where f is the Coriolis parameter, g is the acceleration due to gravity, η is the SSH and u and v are the geostrophic velocities. We assume the geostrophic balance is the same in all directions and calculate the velocity in the x-direction. For the MSS 1996-2002, we take the difference between the gyre's maximum SSH (74°N, 145°W) and the SSH at the edge (~70°N), on the same meridian, to find $\frac{\partial \eta}{\partial x}$. Substituting into equation 2 gives v=1.90±0.1 cms^{-1}. The position of the maximum SSH is the same in the MSS for 2002-2010 as in 1996-2002, therefore we calculated the gradient in the trend between 2002-2010 between the same points defined above, to compute the change in the geostrophic velocity per year. Multiplying by eight (the number of years in the latter half of our time period) gives an increase in the geostrophic velocity of 3.60±0.03 cms^{-1}. Adding this to the geostrophic velocity during the first half of the time period gives 5.50±0.1 cms^{-1}.

The uncertainty in the velocity is estimated by propagating the uncertainty in SSH through equation (2) (see supplementary information).

Freshwater volume change

To calculate the freshwater volume change (ΔFW) we represent each grid cell by a column of water composed of two homogeneous layers with lighter water (density ρ_1) overlying denser water (density ρ_2). The change in water mass at the base of the column (Δm) is

$$\Delta m = \rho_1 \eta - \rho_1 z + \rho_2 z \tag{4}$$

where η is the displacement of the surface (change in SSH), z is the displacement of the interface between ρ_1 and ρ_2, ρ_1=1022 kgm^{-3} and ρ_2=1028 kgm^{-3} (values are for the Canada Basin from figure 2 in[28]). The change in thickness (Δh) of the upper layer is

$$\Delta h = \eta - z \tag{5}$$

Solving equation (4) for z and substituting into (5) gives

$$\Delta h = \eta\left(1 + \frac{\rho_1}{\rho_2 - \rho_1}\right) - \frac{\Delta m}{\rho_2 - \rho_1} \tag{6}$$

The change in the freshwater content is then

$$\Delta FW = \frac{S_2 - S_1}{S_2} A \sum_{i=0}^{N} \Delta h_i \tag{7}$$

where salinities S_1 and S_2 equal 27.7 and 34.7 respectively[28], A is the grid cell area and N is the number of grid cells. To estimate Δm we convert GRACE equivalent water thickness estimates from release 4, University of Texas, Centre for Space Research, 300 km smoothed data (http://grace.jpl.nasa.gov/data/mass/) to mass by multiplying by the density of water (1000 kgm^{-3}). Figure 3 demonstrates that including the mass term makes little difference to our calculation. Therefore, when GRACE data are not available we assume there is no change in mass.

The uncertainty in ΔFW is estimated by propagating the uncertainties in SSH, S_1, ρ_1 and Δm[29] through equation (7) (see supplementary information).

References

1. Carmack, E. C. in *Freshwater Budget of the Arctic Ocean p91-126*, edited by E.L. Lewis (Kluwer, Amsterdam, 2000).

[2] Serreze, M. C. et al., The large-scale freshwater cycle of the Arctic. *Journal of Geophysical Research-Oceans* **111,** (C11) C11010 (2006).

[3] Proshutinsky, A. et al., Beaufort Gyre freshwater reservoir: State and variability from observations. *Journal of Geophysical Research-Oceans* **114**, C00A10 (2009).

[4] McPhee, M. G., Proshutinsky, A., Morison, J. H., Steele, M., and Alkire, M. B., Rapid change in freshwater content of the Arctic Ocean. *Geophys. Res. Lett.* **36**, L10602 (2009).

[5] Rabe, B. et al., An assessment of Arctic Ocean freshwater content changes from the 1990s to the 2006-2008 period. *Deep-Sea Research* **58,** (2), 173-185 (2011).

[6] Holliday, N. P. et al., Arctic Ocean freshwater export reduces while storage increases. *In prep. for JGR* (2011).

[7] Proshutinsky, A., Bourke, R. H., and McLaughlin, F. A., The role of the Beaufort Gyre in Arctic climate variability: Seasonal to decadal climate scales. *Geophys. Res. Lett.* **29,** (23) 2100 (2002).

[8] Curry, R. and Mauritzen, C., Dilution of the northern North Atlantic Ocean in recent decades. *Science* **308,** (5729) 1772-1774 (2005).

[9] Proshutinsky, A. et al., Secular sea level change in the Russian sector of the Arctic Ocean. *Journal of Geophysical Research-Oceans* **109,** (C3) C03042 (2004).

[10] Chambers, D. P., Evaluation of new GRACE time-variable gravity data over the ocean. *Geophys. Res. Lett.* **33,** (17) L17603 (2006).

[11] Rampal, P., Weiss, J., and Marsan, D., Positive trend in the mean speed and deformation rate of Arctic sea ice, 1979-2007. *Journal of Geophysical Research-Oceans* **114**, C05013 (2009).

[12] Spreen, G., Kwok, R., and Menemenlis, D., Trends in Arctic sea ice drift and role of wind forcing: 1992-2009. *Geophys Res Lett* **38,** L19501 (2011).

[13] Comiso, J. C., Parkinson, C. L., Gersten, R., and Stock, L., Accelerated decline in the Arctic Sea ice cover. *Geophys. Res. Lett.* **35,** (1) L01703 (2008).

[14] Giles, K. A., Laxon, S. W., and Ridout, A. L., Circumpolar thinning of Arctic sea ice following the 2007 record ice extent minimum. *Geophys. Res. Lett.* **35,** (22) L22502 (2008).

[15] Kwok, R. and Rothrock, D. A., Decline in Arctic sea ice thickness from submarine and ICESat records: 1958-2008. *Geophys Res Lett* **36**, L15501 (2009).

[16] Andreas, E. L. et al., Parametrizing turbulent exchange over summer sea ice and the marginal ice zone. *Quarterly Journal of the Royal Meteorological Society* **136** (649), 927-943 (2010).

[17] Andreas, E. L. et al., Parametrizing Turbulent Exchange over Sea Ice in Winter. *Journal of Hydrometeorology* **11** (1), 87-104 (2010).

[18] Dickson, R., Meincke, J., Malmberg, S-A., and Lee, A. J., The "Great Salinity Anomaly" in the Northern North Atlantic 1968-1982. *Progress in Oceanography* **20**, 103-151 (1988).

[19] Bindoff, N.L. et al., in *Climate Change 2007: The Physical Science Basis, Contribution of Working Group I to the Fourth Assessment Report of the Intergovernmental Panel on Climate Change*, edited by S. Solomon et al.

(Cambridge University Press, Cambridge United Kingdom and New York NY, USA, 2007).

[20] Belkin, I. M., Propagation of the "Great Salinity Anomaly" of the 1990s around the northern North Atlantic. *Geophys. Res. Lett.* **31,** (8) L08306 (2004).

[21] Peacock, N. R. and Laxon, S. W., Sea surface height determination in the Arctic Ocean from ERS altimetry. *Journal of Geophysical Research-Oceans* **109,** (C7) C07001 (2004).

[22] Kwok, R. and Morison, J., Dynamic topography of the ice-covered Arctic Ocean from ICESat. *Geophys. Res. Lett.* **38**, L02501 (2011).

[23] Pavlis, N. K., Holmes, S., Kenyon, S., and Factor, J. K., presented at the EGU2008-A-01891, 2008 (unpublished).

[24] Kalnay, E. et al., The NCEP/NCAR 40-year reanalysis project. *Bulletin of the American Meteorological Society* **77,** (3) 437-471 (1996).

[25] Makshtas, A. et al., Atmospheric forcing validation for modelling the central Arctic. *Geophys. Res. Lett.* **34,** (20) L20706 (2007).

[26] Bromwich, D. H. and Wang, S. H., Evaluation of the NCEP-NCAR and ECMWF 15- and 40-Yr Reanalyses using rawinsonde data from two independent Arctic field experiments. *Monthly Weather Review* **133,** (12) 3562-3578 (2005).

[27] Gill, A. E., *Atmosphere-Ocean Dynamics Ch. 7* (Academic Press, 1982).

[28] Toole, J. M. et al., Influences of the ocean surface mixed layer and thermohaline stratification on Arctic Sea ice in the central Canada Basin. *Journal of Geophysical Research-Oceans* **115**, C10018 (2010).

[29] Morison, J., Wahr, J., Kwok, R., and Peralta-Ferriz, C., Recent trends in Arctic Ocean mass distribution revealed by GRACE. *Geophys. Res. Lett.* **34**, (7) L07602 (2007).

All correspondence regarding this Letter should be directed to Dr. Katharine Giles. (katharine.giles@ucl.ac.uk)

Acknowledgements

Funding for this work was provided by a fellowship from Natural Environment Research Council and by the National Centre for Earth Observation. Radar altimetry data was provided by the European Space Agency.

Author Contributions

K.A.G., S.W.L., D.J.W and S.B. discussed results and commented on the manuscript. K.A.G lead the analysis, development of the paper and integration of the results. A.L.R. processed the ESA data to provide raw SSH estimates.

Figure 1| Arctic Ocean mean sea surface and trends in sea surface height and the wind field curl (1995-2010). a, Arctic Ocean mean sea surface: Constructed from 15 years of satellite radar altimetry data and calculated with respect to the EGM08 geoid. The Beaufort Gyre is the yellow/orange dome in the Western Arctic. **b**, Trend in sea surface height calculated from satellite radar altimetry. **c**, Trend in the wind field curl calculated from NCEP/NCAR Reanalysis data.

Figure 2| Variability of the sea surface height anomaly and wind field curl anomaly over the Western Arctic. SSH anomaly, taken with respect to the 15-year mean sea surface (figure 1a). The error bar next to the SSH anomaly axis is the 1 sigma uncertainty (± 0.7 cm). Data between September 1995 and September 2002 are from ERS-2 and between October 2002 and September 2010 are from Envisat. The wind field curl anomaly is with respect to the 15 year mean and its error bar marks 10% of the mean wind field curl over the Western Arctic (± 1 ms^{-2}). See figure 3 for map inset showing the Western Arctic region, marked by the grey area.

Figure 3| Change in Western Arctic freshwater content 1995-2010. The asterisks show the change in the freshwater content if the GRACE data are not used in the calculation. Error bars are the 1-sigma uncertainty. Map inset shows the Western Arctic region, marked by the grey area.

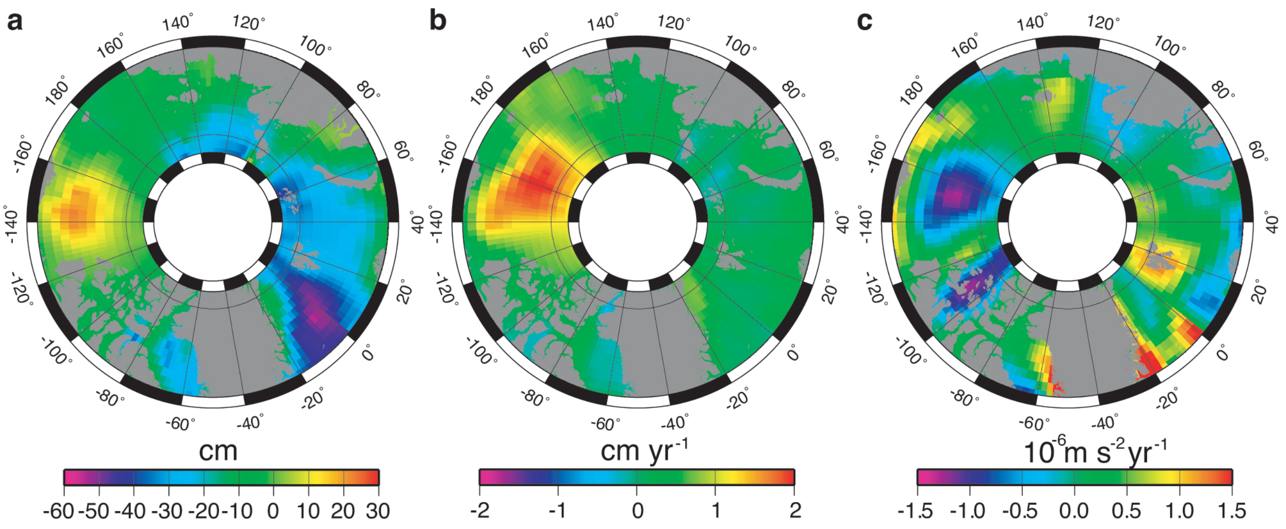

a
b
c
cm
cm yr-1
10-6m s-2yr-1
-60 -50 -40 -30 -20 -10 0 10 20 30
-2 -1 0 1 2
-1.5 -1.0 -0.5 0.0 0.5 1.0 1.5

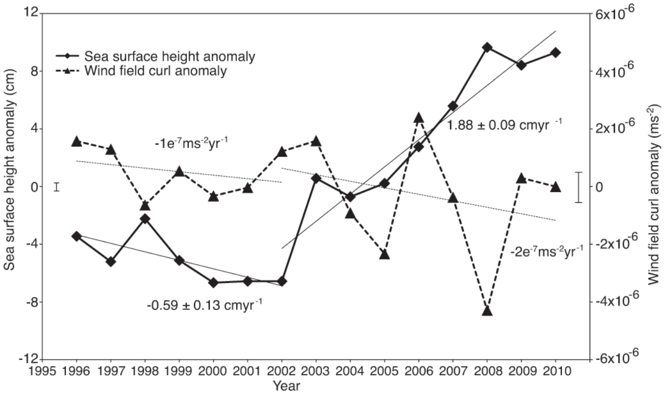

Sea surface height anomaly
Wind field curl anomaly
Sea surface height anomaly (cm)
Wind field curl anomaly (ms^{-2})
Year
$-1e^{-7}ms^{-2}yr^{-1}$
1.88 ± 0.09 $cmyr^{-1}$
$-2e^{-7}ms^{-2}yr^{-1}$
-0.59 ± 0.13 $cmyr^{-1}$
12
8
4
0
-4
-8
-12
$6x10^{-6}$
$4x10^{-6}$
$2x10^{-6}$
0
$-2x10^{-6}$
$-4x10^{-6}$
$-6x10^{-6}$
1995
1996
1997
1998
1999
2000
2001
2002
2003
2004
2005
2006
2007
2008
2009
2010

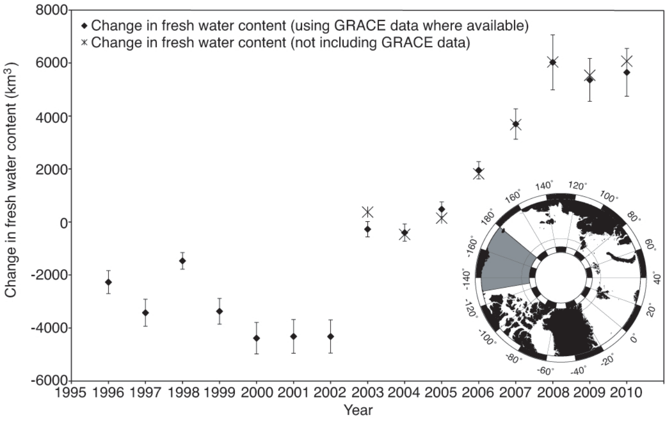

Change in fresh water content (using GRACE data where available)
Change in fresh water content (not including GRACE data)
Change in fresh water content (km^3)
8000
6000
4000
2000
0
-2000
-4000
-6000
1995
1996
1997
1998
1999
2000
2001
2002
2003
2004
2005
2006
2007
2008
2009
2010
Year
140°
120°
160°
100°
180°
80°
-160°
60°
-140°
40°
-120°
20°
-100°
0°
-80°
-20°
-60°
-40°

Supplementary Information for "Western Arctic Ocean freshwater storage increased by wind-driven spin-up of the Beaufort Gyre" by Giles *et al.*,

katharine.giles@ucl.ac.uk

1. Methods

To estimate an elevation from a specular echo returned from a lead in the sea ice pack we fit an empirically derived model to the echo[1]. Over the open ocean (during the Arctic summer) standard elevation data from the European Space Agency (ESA) products were used. Our correction for the bias between open ocean and lead sea surface height (SSH) estimates, which results from using different processing techniques, is described in detail below. In correcting for this bias we also remove any potential bias in the lead elevation resulting from the echo shape differing from the empirical modal we fit to the data.

For ERS-2, the orbits were provided by the Delft University of Technology and were based on the DGM-E04 gravity model[2] and for Envisat, the standard precision orbits from ESA were used. Satellite altitudes were referenced to an ellipsoid of the Earth based on the WGS-84 reference system. The following corrections were applied to both ERS and Envisat data: ionospheric delay using the GIM model (http://iono.jpl.nasa.gov/gim.html), wet and dry components of the troposphere delay (computed from 6-hourly NCEP surface pressure, humidity and temperature grids), long term instrument drift due to the drift in the frequency of the ultra stable oscillator[3], ocean tides as detailed in[4] and the inverted barometer effect using the MOG 2D model[5].

1.2 Removing the lead/open ocean bias

To calculate a trend in the SSH in a grid cell we require that each grid cell contains data from all months in the year, for every year, to avoid potential variations in the seasonal cycle affecting the calculation. Our analysis therefore requires data from both ice covered and open ocean areas as, during August, September and October, as there are significant areas of the Western Arctic that are ice free. There is a bias between elevation estimates from the open ocean and from leads as different models are used to fit to the echoes and provide an elevation estimate.

The bias between open ocean and lead SSH estimates was calibrated using data from the ice edge (lead elevations are lower than ocean elevations). For both satellites the distribution of the difference between ocean and lead elevations is approximately Gaussian with a mean, standard deviation and standard error of 15, 11 and 0.2 cm for ERS-2 and 4, 7 and 0.4 cm for Envisat respectively. We add the mean difference to the lead elevations to correct for this bias. As the returns from leads and the ocean cannot not be acquired from exactly the same point, variability in the difference between the them is due in part to variations in the SSH between the ice covered and ice free areas. We take the larger standard error of 0.4 cm as an estimate of the uncertainty when correcting for this bias.

To check the lead/open ocean bias correction we compared the annual SSH and trends over the Western Arctic from lead only data and from combining both lead and the open ocean data. We removed the months of August, September and October in each of the annual averages (for both data sets) to ensure that we had lead data covering all of the Western Arctic during every month in our average during every year. The differences between the lead only and lead plus open ocean annual average

SSH are at the millimetre scale and the trends agree to 3%. Therefore we do not think that this bias affects our trend calculation after we have applied the correction.

It is possible to get specular return from young, undeformed, snow-free ice in leads. This ice type of ice could have an elevation of up to few cm's above the sea surface. We would expect that the effect of sampling new ice would increase the variability of our data as the probability of the satellite sampling an open lead or newly refrozen lead is the same. If new ice were causing our elevation estimates to be biased high then this bias would be removed when we calibrate the lead data with the open ocean data and if there were a trend towards increased returns from new ice would see that in our ice/open ocean calibration, which we do not.

1.3 Cross-calibrating ERS-2 and Envisat

ERS-2 was launched in 1995 and operated fully until June 2003 when one of its tape recorders failed. Following this, ERS-2 provided limited spatial coverage of the Arctic until October 2006. Envisat was launched in 2002, into the same orbit as ERS-2, 30 minutes ahead. There are 9 months (October 2002 to June 2003) where there is full coverage of the Arctic from both satellites. The altimeters onboard ERS-2 and Envisat employ the same main frequency, bandwidth, antenna beamwidth and range resolution. The primary difference between the two altimeters lies in the algorithm used to maintain the surface echo (known as tracking) within the instruments recording system. ERS-2 was designed to track echoes over the ocean. The echoes returned from leads cause the recording window on ERS-2 to oscillate, resulting in the blurring of the echo[4]. In contrast, the Envisat altimeter is designed to track over a wide variety of surfaces and therefore has a recording system that is much more stable for non-ocean echoes, providing a considerable reduction in instrument noise[6].

To cross calibrate the data from ERS-2 and Envisat we compute monthly maps of the SSH (with respect to the geoid) in the Western Arctic between October 2002 and October 2006, sub sampling the Envisat data to match the reduced coverage from ERS-2 after June 2003. We then calculate a running mean over 12 months of data as we are presenting annual averages in the manuscript (supplementary information figure 1). We only include grid cells in each average that contain data from both satellites for each of the 12 months that comprise that annual average (except for those averages that include May 2006 as there is no ERS-2 data for this month, therefore the condition changes to 11 months). Out of the 48 possible gird cells in the Western Arctic each annual average contains at least 10.

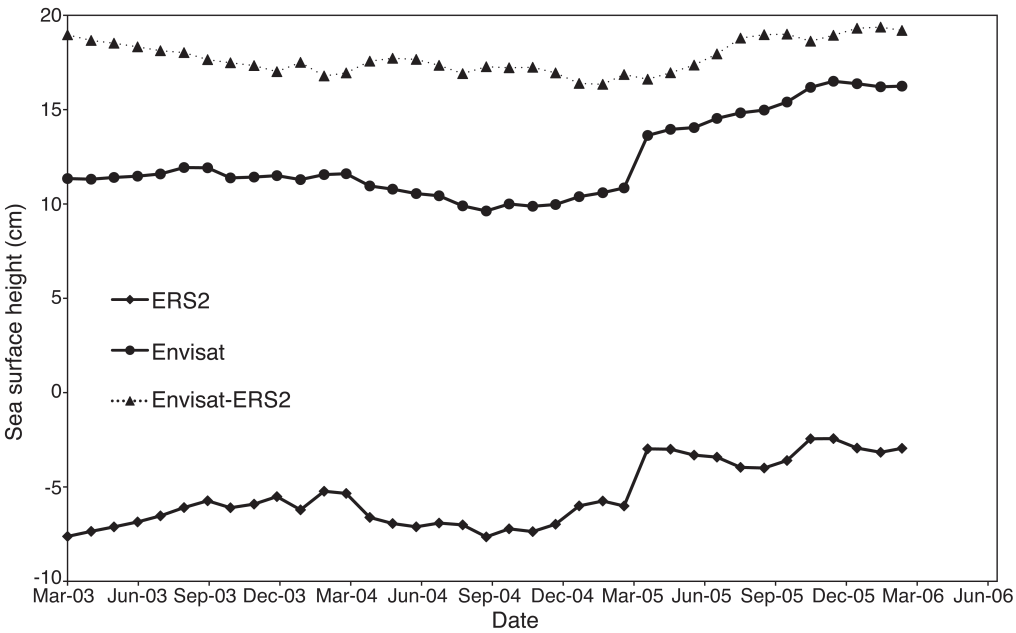

Supplementary Information Figure 1| Cross-calibration of sea surface height from Envisat and ERS-2 over the Western Arctic. Each data point represents an annual average SSH estimate plotted at the centre month e.g. the data point at March-03 is the average between October-02 and September-03. The 1-sigma uncertainties in the annual average SSH and difference between the satellites are 0.5 cm and 0.7 cm respectively.

The mean difference is 18 cm with a standard deviation and standard error of 0.9 and 0.2 cm respectively. We add 18 cm to the ERS2 elevation estimates to correct for the bias between the satellites and take the standard error of 0.2 cm as an estimate of the uncertainty in correcting for this bias

Independently, the instrumental drift in Envisat is calibrated to within 0.5 mm yr^{-1} in range[7] whilst the trend in ERS agrees within 0.5 mm yr^{-1} with the TOPEX radar altimeter, which is itself calibrated[8] to 1 mm yr^{-1}. Considering these calibrations, and that the trend in the SSH we observe over the Arctic region is not uniform, the trend we observe in the Western Arctic is not due to instrument drift.

1.4 Estimating the uncertainty in the SSH

To estimate the uncertainty in the SSH due to measurement, orbit, tidal, instrument noise and atmospheric propagation errors we use the mean RMS variability of 7.3 cm in the Canada basin[4] derived from two years of ERS-2 SSH measurements. Since all of these de-correlate for the different orbits within each grid cell we divide by the square root of the number of orbits (n) in a grid cell at 70°N. To account for the uncertainty resulting from the corrections for the lead/open ocean bias and the ERS-2/Envisat bias we used the standard error (0.4 and 0.2 cm respectively) for each bias correction as described above and add these uncertainties in quadrature to the RMS variability.

For a single grid cell for an annual average, σ_{annual}=0.8 cm (n=125) and the 15-year mean σ_{mean15}=0.5 cm (n=1875). Therefore, the error in the SSH anomaly for a single grid cell is $\sigma_{anomaly}$=0.9 cm. The uncertainty in the SSH averaged over the Western Arctic (n=1452) is σ_{annual_WA}=0.5 cm, σ_{mean15_WA}=0.4 cm and $\sigma_{anomaly\_WA}$=0.7

cm. The uncertainties given for the trends in the text are the 1-sigma uncertainties for the estimate of each trend.

1.5 Estimating the uncertainty in the geostrophic velocity

The uncertainty in the geostrophic velocity, during the first half of our time period (1996-2002), calculated between two points in the Beaufort Gyre is estimated from

$$\sigma_v^2 = 2\sigma_{mean7}^2\left(\frac{g}{\Delta x f}\right)^2 \qquad (1)$$

where the uncertainty in the 7-year MSS is σ_{mean7}=0.5 cm (n=875) and Δx is the distance between the centre and edge of the gyre. The uncertainty in the total increase in the geostrophic velocity during the second half of our time series is estimated using equation 1 and by replacing σ_{mean7} with the uncertainty in the trend for an individual grid cell σ_{trend}=0.12 cm (this value is the uncertainty in fitting a linear trend to the sea surface height anomaly in a single grid cell with uncertainty $\sigma_{anomaly}$=0.9 cm).

1.6 Estimating the uncertainty in the change in the fresh water volume

The uncertainty in the change in the fresh water content is estimated by first calculating the uncertainty in *Δh* (the change in thickness of the upper layer) for a single grid cell

$$\sigma_{\Delta h}^2 = \sigma_\eta^2\left(1+\frac{\rho_1}{\rho_2-\rho_1}\right)^2 + \sigma_{GRACE}^2\left(\frac{\rho}{\rho_2-\rho_1}\right)^2 + \sigma_{\rho_1}^2\left(\eta\left(\frac{\rho_1}{(\rho_2-\rho_1)^2}+\frac{1}{(\rho_2-\rho_1)^2}\right)-\frac{\Delta m}{(\rho_2-\rho_1)^2}\right)^2 \qquad (2)$$

where ρ is the density of water (1000 kg m^{-3}), ρ_1 and ρ_2 are the densities in the upper and lower layers, Δm is the change in mass and η is the change in the SSH. The uncertainty in the change in the SSH is σ_η=0.9 cm, the uncertainty in the GRACE estimate of the change in the water thickness σ_{GRACE}=2.8 cm[9] and the uncertainty in the density of the upper layer $\sigma_{\rho_1} = 7$ Kg m^3. The uncertainty in the freshwater estimate is then calculated from

$$\sigma_{\Delta FW}^2 = \sum_{i=0} \sigma_{\Delta h_i}^2 \left(A \frac{S_2 - S_1}{S_2} \right)^2 + \sigma_{S_1}^2 \left(\frac{A \Delta h_i}{S_2} \right) \tag{3}$$

where A is the grid cell area and N is the total number of grid cells and S_1 and S_2 are the salinities of the upper and lower layers. The uncertainty in the top layer salinity is $\sigma_{S_1} = 9$ psu. The uncertainty estimates for the top layer density and salinity values are the maximum range of mixed layer densities/salinities from measurements in the Canada Basin in April and September 2007 and April 1975[10]. We take these values to be an upper bound on the range of salinities as comparison of summer and winter salinity and density maps from climatological averages from the Polar science centre Hydrographic Climatology (PHC version 3.0[11]) (Supplementary Information Figure 2) give maximum differences of 1.8 kg m^{-3} (density) and 2.1 psu (salinity) in the Western Arctic.

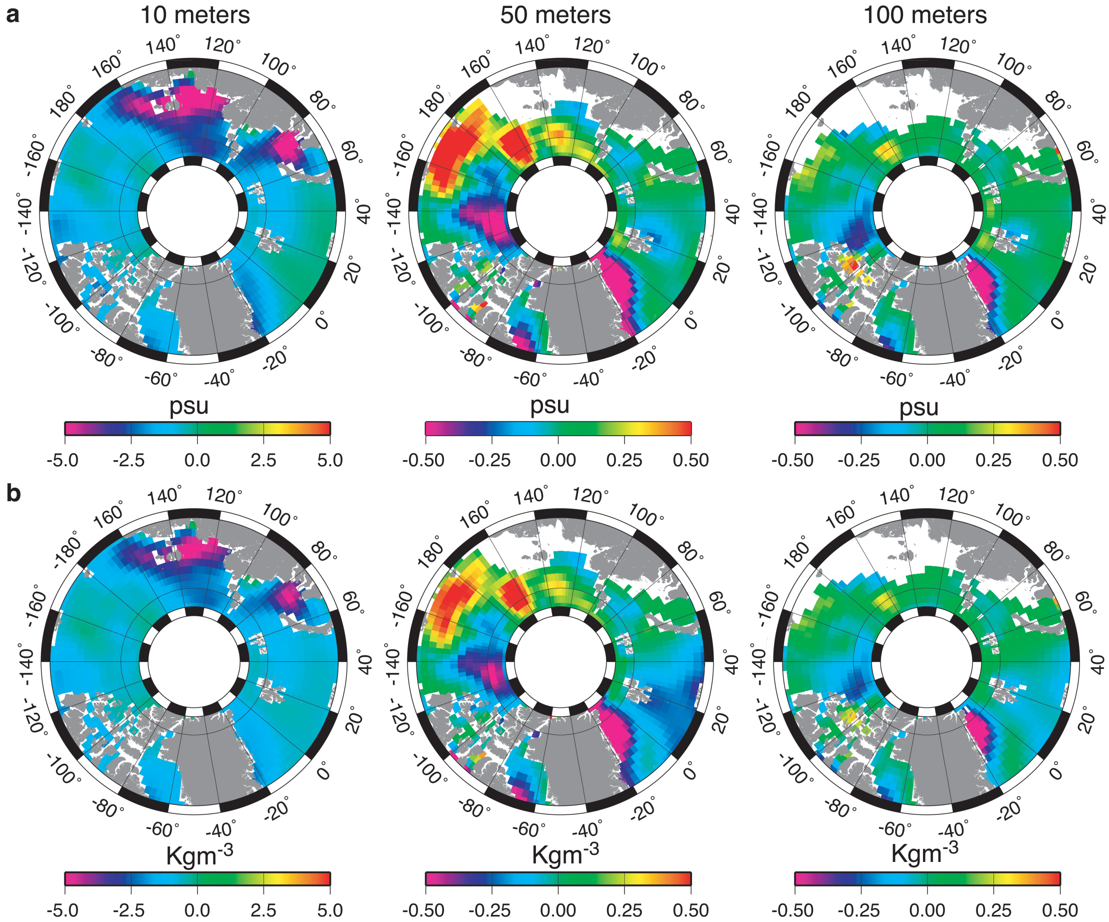

Supplementary Information Figure 2| Seasonal difference in salinity and density at 10, 50 and 100 meters depth from the Polar Science Center Hydrographic Climatology. Summer minus winter a) salinity and b) density. Note that the scales for the 10 meters plots are different to those for the 50 and 100 meter plots.

We have only considered the uncertainty in the density and salinity of the upper layer as variability in density and salinity in the lower layer is small in comparison. Supplementary Information Figure 2 show that the maximum seasonal difference in salinity and density in the Western Arctic at 10 m depth is 2.1 psu and 1.8 Kgm^{-3} while at 50 m and 100 m the difference is 3 to 9 times smaller (0.7 and 0.3 psu, and 0.5 and 0.2 Kg m^{-3} respectively). Including the uncertainty in the lower layer salinity and density in our uncertainty estimate for the change in the fresh water volume does not change its value after rounding up to the nearest thousand km^3.

1.7 Estimating the uncertainty in the wind field curl

The NCEP/NCAR Reanalysis data wind speed values have been validated in the Arctic by comparison to observations from drifting stations between 1954 and 2006[12] and in the Western Arctic by observations made during the LeadEx campaign in and around an ice camp in the Beaufort Sea during March and April 1992[13].

The Arctic wide validation found correlation coefficients between 0.68 and 0.77 and differences in wind speed between -0.3 to 0.8 ms^{-1} (average wind speed is 3.5-6 ms^{-1}), over our observational period and the best results were obtained in the Beaufort Gyre region[12]. The data gathered during LeadEx showed correlation co-efficients (r) of 0.9 and 0.79 in the u and v components of wind, and 0.84 for wind speed and bias's of 0.45, -1.2 and -0.6 ms^{-1} for the u, v and wind speed respectively[13]. Considering these data we estimate an uncertainty in the wind speed of 10%.

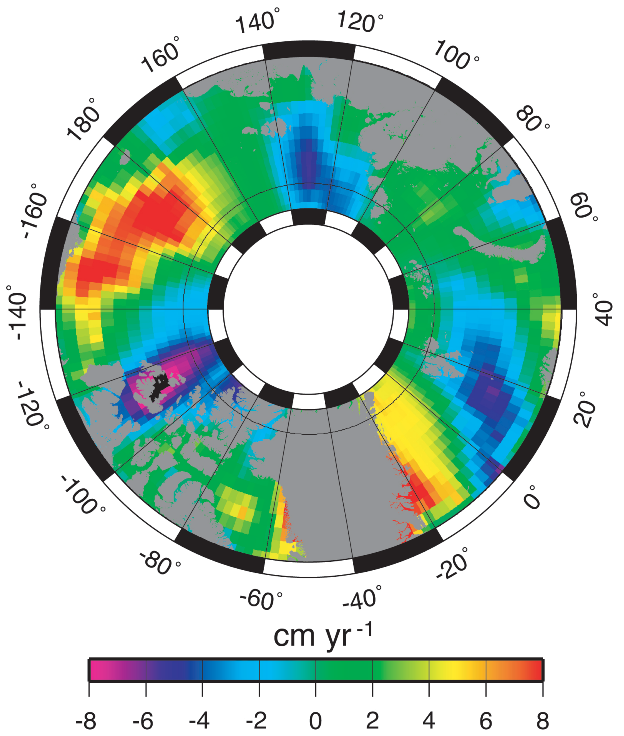

Supplementary Information Figure 3| Trend in the wind speed anomaly 1995-2010. Calculated from NCEP/NCAR Reanalysis data.

The estimate the uncertainty in the wind field curl would require some external knowledge of the error in the spatial gradient of the wind field, which does not exist. However, we investigated the trend in the wind speed (supplementary information figure 3) and found it to be substantially similar to the trend in the wind field curl. Therefore, we also assume a 10% uncertainty in the wind field curl.

Supplementary References

1 Giles, K. A. et al., Combined airborne laser and radar altimeter measurements over the Fram Strait in May 2002. *Remote Sens. Environ.* **111**, (2-3), 182-194 (2007).

[2] Scharroo, R. and Visser, P., Precise orbit determination and gravity field improvement for the ERS satellites. *J. Geophys. Res.-Oceans* **103**, (C4), 8113-8127 (1998).

[3] Scharroo, R., Schrama, E., Naeije, M., and Benveniste, J., presented at the ERS-ENVISAT Symposium, Gothenburg, Sweden, 16-20 October 2000, 2000.

[4] Peacock, N.R. and Laxon, S.W., Sea Surface Height Determination in the Arctic Ocean from ERS Altimetry. *J. Geophys. Res.* **109**, (C7) C07001 (2004).

[5] Carrere, L. and Lyard, F., Modeling the barotropic response of the global ocean to atmospheric wind and pressure forcing - comparisons with observations. *Geophys. Res. Lett.* **30,** (6) 1275 (2003).

[6] Roca, M., Laxon, S., and Zelli, C., The EnviSat RA-2 Instrument Design and Tracking Performance. *IEEE T. Geosci. Remote Sens.* **47**, (10), 3489-3506 (2009).

[7] Leuliette, E. W. and Miller, L., Closing the sea level rise budget with altimetry, Argo, and GRACE. *Geophys. Res. Lett.* **36,** L04608 (2009).

[8] Cazenave, A., A., K. Dominh, Gennero, M. C., and Ferret, B., Global mean sea level changes observed by TOPEX-Poseidon and ERS-1. *Phys. Chem. Earth* 23(9–10), 1069-1075 (1998).

[9] Morison, J., Wahr, J., Kwok, R., and Peralta-Ferriz, C., Recent trends in Arctic Ocean mass distribution revealed by GRACE. *Geophys. Res. Lett.* **34**, (7) L07602 (2007).